



**HAL**  
open science

## Effects of global climate oscillations on intermonthly to interannual variability of sea levels along the English Channel Coasts (NW France)

Imen Turki, Nicolas Massei, Benoît B. Laignel, Hassan Shafiei

► **To cite this version:**

Imen Turki, Nicolas Massei, Benoît B. Laignel, Hassan Shafiei. Effects of global climate oscillations on intermonthly to interannual variability of sea levels along the English Channel Coasts (NW France). *Oceanologia*, 2020, 62 (2), pp.226-242. 10.1016/j.oceano.2020.01.001 . hal-02886424

**HAL Id: hal-02886424**

**<https://hal.science/hal-02886424>**

Submitted on 16 Apr 2021

**HAL** is a multi-disciplinary open access archive for the deposit and dissemination of scientific research documents, whether they are published or not. The documents may come from teaching and research institutions in France or abroad, or from public or private research centers.

L'archive ouverte pluridisciplinaire **HAL**, est destinée au dépôt et à la diffusion de documents scientifiques de niveau recherche, publiés ou non, émanant des établissements d'enseignement et de recherche français ou étrangers, des laboratoires publics ou privés.



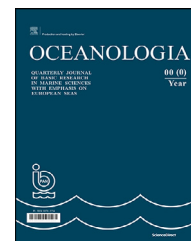
Distributed under a Creative Commons Attribution - NoDerivatives 4.0 International License



Available online at [www.sciencedirect.com](http://www.sciencedirect.com)

ScienceDirect

journal homepage: [www.journals.elsevier.com/oceanologia](http://www.journals.elsevier.com/oceanologia)



ORIGINAL RESEARCH ARTICLE

# Effects of Global Climate Oscillations on Intermonthly to Interannual Variability of Sea levels along the English Channel Coasts (NW France)

Imen Turki\*, Nicolas Massei, Benoit Laignel, Hassan Shafiei

UMR CNRS 6143 – Continental and Coastal Morphodynamics ‘M2C’, University of Rouen, Mont-Saint-Aignan Cedex, France

Received 25 May 2019; accepted 20 January 2020

Available online 5 February 2020

## KEYWORDS

Sea level;  
Extreme surges;  
Multiscale variability;  
Storms;  
Climate oscillations;  
Multiresolution  
analysis

**Summary** This work examines the multiscale variability in sea level along the English Channel coasts (NW France) using a wavelet multiresolution decomposition of water level values and climate oscillations in order to gain insights in the connection between the global atmospheric circulation and the local-scale variability of the monthly extreme surges. Changes in surges have exhibited different oscillatory components from the intermonthly (~3–6-months) to the interannual scales (~1.5-years, ~2–4-years, ~5–8-years) with mean explained variances of ~40% and ~25% of the total variability respectively. The correlation between the multiresolution components of surges and 28 exceptional stormy events with different intensities has revealed that energetic events are manifested at all timescales while moderate events are limited to short scales.

By considering the two hypotheses of (1) the physical mechanisms of the atmospheric circulation change according to the timescales and (2) their connection with the local variability improves the prediction of the extremes, the multiscale components of the monthly extreme surges have been investigated using four different climate oscillations (Sea Surface Temperature (SST), Sea-Level Pressure (SLP), Zonal Wind (ZW), and North Atlantic Oscillation (NAO)); results show statistically significant correlations with ~3–6-months, ~1.5-years, ~2–4-years, and ~5–8-years, respectively. Such physical links, from global to local scales, have been

\* Corresponding author at: Imen Turki, UMR CNRS 6143 – Continental and Coastal Morphodynamics ‘M2C’, University of Rouen, 76821 Mont-Saint-Aignan Cedex, France.

*E-mail addresses:* [imen.turki@univ-rouen.fr](mailto:imen.turki@univ-rouen.fr) (I. Turki), [nicolas.massei@univ-rouen.fr](mailto:nicolas.massei@univ-rouen.fr) (N. Massei), [benoit.laignel@univ-rouen.fr](mailto:benoit.laignel@univ-rouen.fr) (B. Laignel), [hassan.shafiei@univ-rouen.fr](mailto:hassan.shafiei@univ-rouen.fr) (H. Shafiei).

Peer review under the responsibility of Institute of Oceanology of the Polish Academy of Sciences.



Production and hosting by Elsevier

<https://doi.org/10.1016/j.oceano.2020.01.001>

0078-3234/© 2020 Institute of Oceanology of the Polish Academy of Sciences. Production and hosting by Elsevier B.V. This is an open access article under the CC BY-NC-ND license (<http://creativecommons.org/licenses/by-nc-nd/4.0/>).

considered to model the multiscale monthly extreme surges using a time-dependent Generalized Extreme Value (GEV) distribution. The incorporation of the climate information in the GEV parameters has considerably improved the fitting of the different timescales of surges with an explained variance higher than 30%. This improvement exhibits their nonlinear relationship with the large-scale atmospheric circulation.

© 2020 Institute of Oceanology of the Polish Academy of Sciences. Production and hosting by Elsevier B.V. This is an open access article under the CC BY-NC-ND license (<http://creativecommons.org/licenses/by-nc-nd/4.0/>).

## 1. Introduction

With the present context of global climate change, most of researchers claim that the sea-level variability and the increase of storminess are considered significant hazards for several low-lying coastal communities (e.g. Hanson et al., 2011; Nicholls et al., 2011). Hence, many efforts have been devoted to better understand the natural processes driving the multiscale variability of the extreme sea levels to produce a more accurate estimation of their fluctuations and ensuring reliable coastal risk assessments. This challenge serves as the basis for implementing an appropriate adaptation strategy reducing the disastrous risks of the coastal flooding. The sea-level changes, encompassing cyclical seasonal components superimposed on long-term trends and stochastic variability, are one of the most important physical processes affecting the coastal systems. These changes are due to the frequent temporal shifts linked to the nonlinear, stochastic, or transient effects of external factors such as the global climate patterns (Pasquini et al., 2008).

Changes in sea levels are largely driven by the large-scale atmospheric and oceanic circulation patterns operating on intermonthly and interannual timescales. Moreover, studying the links of the sea-level variability with the climate teleconnections, related to prominent atmospheric modes as proxies, is necessary to fully understand the interplay between the climate oscillations and the oceanographic processes (e.g. Dangendorf et al., 2012; Levin, 1992; Yan, 2004; Zampieri et al., 2017). Some works have been implemented to understand and extract the signature of internal climate variability from the observed sea-level patterns (e.g. Dangendorf et al., 2012; Levin, 1992; Yan, 2004; Zampieri et al., 2017) with the aim of contributing in the multiscale sea-level predictions that emerge as urgent priorities in the state-of-the-art climate research.

Large timescale studies around the English Channel (South coast of UK) have been presented in Haigh et al. (2009) work, where changes in the mean sea levels have been investigated by the use of hourly sea-level records extended by data archaeology. They have found that mean sea-level trends vary between 0.8 and 2.3 mm/year around the Channel. A new approach of spectral analysis has been used by Turki et al. (2015a) to investigate the annual and the intermonthly changes of the sea level along the English Channel coasts (NW France). Such multiscale changes have been linked to a combination of meteorological and North Atlantic Oscillation (NAO) climate drivers, involving several processes over a wide range of spatial and temporal scales.

Being an alarming problem for the coastal vulnerability, extreme events have gained the attention of the scientists who have reported the dynamics (e.g., Haigh et al., 2010; Idier et al., 2012; Masina and Lamberti, 2013; Tomasin and Pirazzoli, 2008; Turki et al., 2019) and the projections (e.g., Vousdoukas et al., 2017) of extreme sea levels considering the stationary and the nonstationary contributions from tides, waves, sea-level-rise components (e.g., Brown et al., 2010; Idier et al., 2017), and large-scale climate oscillations (e.g., Colberg et al., 2019; Turki et al., 2019).

A number of studies have examined the relationship between the global atmospheric patterns and the local sea levels to estimate sea-level extreme values by the use of nonstationary statistical approaches. Regional studies of extreme sea levels have been conducted in various works using different methodologies; the most common of them is related to the Generalized Extreme Value (GEV) models. A review of extreme analyses has been performed by Mendez and Woodworth (2010); they applied a nonstationary extreme value model to the monthly maxima with a special focus on NAO to study the variability of the extreme sea levels along the European coasts. Masina and Lamberti (2013) have used a nonstationary GEV model to demonstrate a coherent behavior between the regional and the global scales from a detailed analysis of the annual mean sea-level evolution in the Adriatic sea with the NAO and AO (Arctic Oscillation) indices; they have suggested that the increase in the extreme water levels since the 1990s is related to the changes in the wind regime and the intensification of Bora and Sirocco winds after the second half of the 20<sup>th</sup> century.

In the English Channel, the extreme sea levels have been addressed by several works (e.g. Haigh et al., 2010; Idier et al., 2012; Tomasin and Pirazzoli, 2008; Turki et al., 2019) with the aim of investigating their dynamics at different timescales and their connections to the atmospheric circulation patterns.

Haigh et al. (2010) investigated the interannual and the interdecadal extreme surges in the English Channel and their strong relationship with the NAO index. Their results showed weak negative correlations throughout the Channel and strong positive correlations at the boundary along the Southern North Sea. Using a numerical approach, Idier et al. (2012) studied the spatial evolution of some historical storms in the Atlantic Sea and their dependence on tides.

Recently, Turki et al. (2019) have examined the multiscale variability of the sea-level changes in the Seine Bay (NW France) in relation with the global climate oscillations from the SLP composites; they have demonstrated dipolar patterns of high-low pressures suggesting positive and

negative anomalies at the interdecadal and the interannual scales, respectively.

Despite these important advances, no particular studies exist on sea-level dynamics and extreme events linked to the large-scale climate oscillations along the English Channel coastlines. The aforementioned works of Turki et al. (2015a, 2019) have focused on the multiscale sea-level variability along the French coasts related to the NAO and the Sea-Level Pressure (SLP) patterns; however, they have not addressed the regional behavior of the extreme sea levels in relation with the global climate oscillations.

The present contribution aims to investigate the regional dynamics of the sea level and the extreme events in some selected English Channel coasts (NW France) and seeks to understand their multiscale connection to the large-scale atmospheric circulation. A spectral approach based on the continuous and multi-resolution wavelet techniques has been used herein in order to (i) visualize and investigate the spectral content of the sea levels on intermonthly to the interannual scales, (ii) identify the links between the sea-level fluctuations and the increase of the historical storm events, (iii) quantify the multiscale changes in the monthly maxima of extreme surges and their connection with the atmospheric circulation by applying a nonstationary approach using the climate oscillations.

The rest of the paper is organized into four sections: Section 2 gives a description of the data sources and the methodological approach used to investigate the multiscale variability of the sea level with the atmospheric circulation. Local-scale changes in sea levels along the English Channel and their connection with the climate oscillations have been addressed and discussed in sections 3 and 4, respectively. Finally, all findings are summarized and concluded in Section 5.

## 2. Data and methods

### 2.1. Sea-level and climate datasets

The present research is focused on the Normandy coasts along the Southern side of the English Channel (North of France); it has been conducted in the framework of the French research program ANR RICOCHET and the international project COTEST funded by CNES-TOSCA and related to the future mission Surface Water and Ocean Topography (SWOT).

Sea-level data, obtained from three tide gauge sites, are used in the present study: (1) Dunkirk station which is a few kilometers away from Belgian borders, (2) Le Havre stations situated on the right bank of the estuary of the Seine River, and (3) Cherbourg station located on the Cotentin Peninsula and at the opening of the Atlantic Sea. These stations provide time-series of hourly observations measured between 1964 and 2010. The tide gauges are operated and maintained by the National French Center of Oceanographic Data (SHOM). The observations which correspond to the hydrographic zero level are referenced to zero tide gauge (Fig. 1). The storm events produced in the English Channel largely occurred along Cherbourg, Le Havre, and Dunkirk coasts. The surges in these regions are equal or higher than the

values of 2year return period ( $Re$ ) which represents 1.2 m, 1.3 m, and 1.6 m, respectively (SHOM).

The large-scale atmospheric circulations are represented in the present analysis by four different climate indices which are considered as fundamental drivers in the Atlantic regions: the Sea Surface Temperature (SST), the North Atlantic Oscillation (NAO), the Zonal Wind (ZW) component extracted at 850hPa, and the Sea-Level Pressure (SLP). Monthly time-series of climate index have been provided by the NCEP-NCAR Reanalysis fields<sup>1</sup> with the same period during which the sea-level observations were conducted (i.e. 1964–2010).

### 2.2. Methods

The total sea-level height, resulting from the astronomical and the meteorological processes, exhibits a temporal non-stationarity which is explained by a combination of the effects of the long-term trends in the mean sea level, the modulation by the deterministic tidal component and the stochastic signal of surges, and the interactions between tides and surges. The occurrence of extreme sea levels is controlled by periods of astronomically-generated high tides, in particular, at inter-annual scale when two phenomena of precession cause systematic variation of high tides. The modulation of the tides contributes to the enhanced risk of coastal flooding. Therefore, the separation between tidal and non-tidal signal is an important task in any analysis of sea-level time-series.

By the hypothesis of independence between the astronomical tides and the stochastic residual of surges, the non-linear relationship between the tidal modulation and surges is not considered in the present analysis. Using the classical harmonic analysis, the tidal component has been modeled as the sum of a finite set of sinusoids at specific frequencies to determine the determinist phase/ amplitude of each sinusoid and predict the astronomical component of tides. In order to obtain a quantitative assessment of the non-tidal contribution in storminess changes, technical methods based on MATLAB t-tide package have been used to estimate year-by-year tidal constituents. A year-by-year tidal simulation (Shaw and Tsimplis, 2010) has been applied to the sea-level time-series to determine the amplitude and the phase of tidal modulations using harmonic analysis fitted to 18.61-, 9.305-, 8.85-, and 4.425-year sinusoidal signals (Pugh, 1987). The radiational components have been also considered for the extraction of the stochastic component of surges (Williams et al., 2018). The hourly sea-level measurements present some short gaps (of some days) distributed during the first 30 years (1964–1995) of the total time-series. These gaps, with respect to the total series, represent 2% in Cherbourg and Le Havre and 5% in Dunkirk; they have been processed by the hybrid model for filling gaps developed by Turki et al. (2015b). The model applies a purely statistical approach to the stochastic component of the sea level (residual component) based on Autoregressive Moving Average (ARMA) techniques with introducing SLP in ARMA as a main physical process driving the residual

<sup>1</sup> [http://www.esrl.noaa.gov/psd/data/gridded/data.ncep\\_reanalysis.derived.html](http://www.esrl.noaa.gov/psd/data/gridded/data.ncep_reanalysis.derived.html)

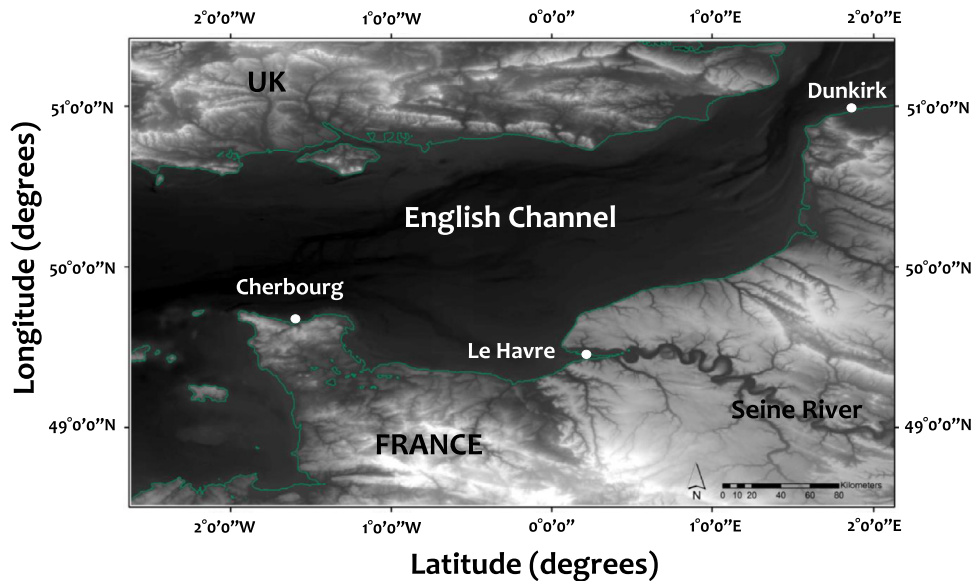


**Figure 1** Geographical location of the study area and the different tide gauges along the Southern English Channel coasts (NW France): Dunkirk, Le Havre, and Cherbourg.

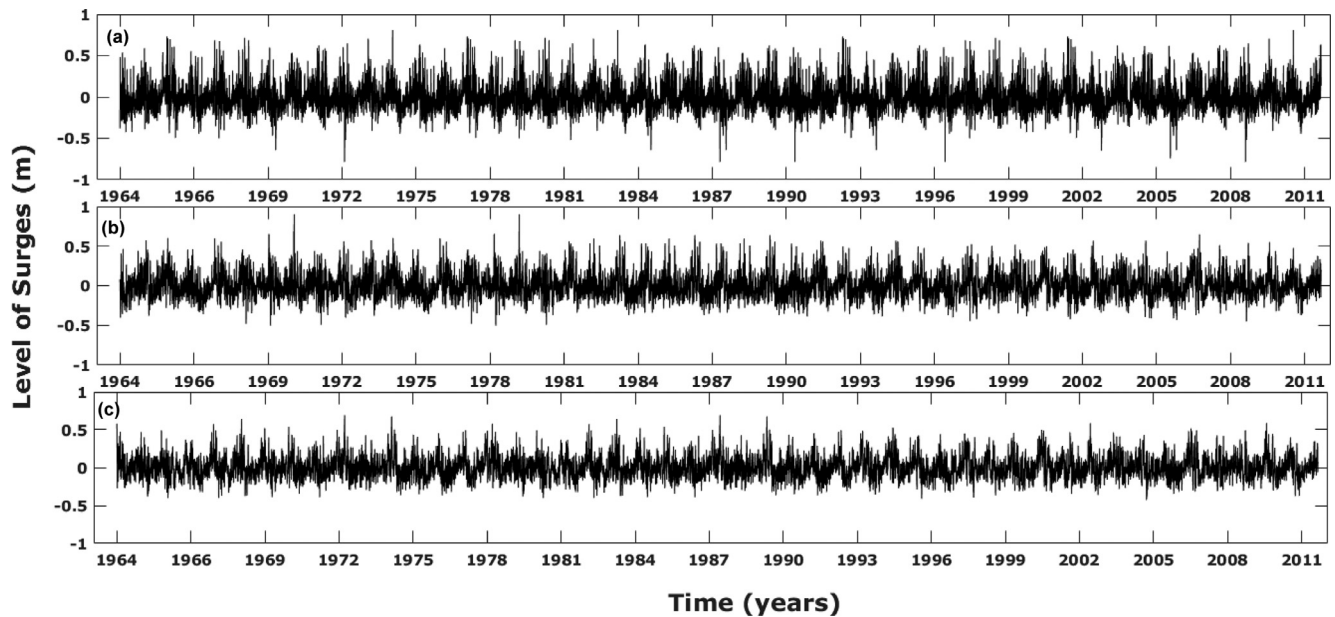


**Figure 2** The hourly surges during the period 1964–2010 in (a) Dunkirk, (b) Le Havre, and (c) Cherbourg.

sea level. They have used this model to process the sea-level records provided by the tide gauges along the Atlantic French coasts. The model has been used also by Turki et al. (2019) for data processing. The total sea level and surges at Dunkirk, Le Havre, and Cherbourg are illustrated in Fig. 2.

The general approach developed herein intends to: (1) identify the main timescales of the variability of the total sea levels and surges, (2) characterize the multiscale relationships between the local-scale hydro-climatological signal of the surges and the historical storm events on large scales, (3) examine the ability of the potential monthly climate predictors (NAO, ZW, SLP, SST) to describe the time-scale decomposition of the monthly extreme surges by identifying the physical link between both variables at each time

scale. Such physical link has been used for a multiscale parameterization of the non-stationary GEV models. Firstly, the hourly hydro-climatological signals (i.e. total sea level and surges) have been analyzed using continuous wavelet transform (CWT) to explore the spectral content of oceanographic signals. The typical scales of the sea-level variability (Turki et al., 2015a, 2019) have been detected from different records.

The CWT is a well-known method that has been used over the past decade for data analysis in hydrology, geophysics, and environmental sciences (Labat, 2005; Sang, 2013; Torrence and Compo, 1998). The continuous wavelet transform produces either a time-scale or time-period with the means of the Fourier transform contour diagram on

which time is indicated on the x-axis, period, or scale on the y-axis, and amplitude (or variance, or power, etc.) on the z-axis.

Secondly, the hourly surges have been decomposed by wavelet multiresolution analysis into different internal components corresponding to different time-scales. Briefly, the multiresolution analysis consists of the iterative filtering of the time-series using a series of low-pass and high-pass filters which eventually produce one high-frequency “rough” component called “wavelet detail” and one lower frequency “coarse” component called “smooth” or “approximation”.

The smooth, produced at each scale, is then subsequently decomposed into a second wavelet detail and a second smooth, the latter is decomposed again in the same way until one last smooth remains and will no longer be decomposed. Summing up all wavelet details and the last smooth (i.e. the lowest-frequency component) gives back the original signal. In summary, the total signal has been separated into a relatively small number of wavelet components from high to low frequencies that altogether explains the variability of the signal; this will be illustrated later using the hourly measurements and the monthly maxima of surges.

Finally and with the aim of addressing the nonstationary behavior of extreme surges, the monthly maxima of the surges have been calculated and decomposed with the multiresolution analysis. Then, a nonstationary extreme value analysis based on the GEV distribution with time-dependent parameters (Coles, 2001) has been implemented to model the series of the monthly maxima surges. There are several GEV families which depend on the shape parameter, e.g. Weibull ( $\varepsilon < 0$ ), Gumbel ( $\varepsilon = 0$ ), and Fréchet ( $\varepsilon > 0$ ). The three parameters of the GEV (i.e. location  $\mu$ , scale  $\psi$ , shape  $\varepsilon$ ) are estimated by the maximum likelihood function.

The nonstationary effect was considered by incorporating the selected climate indices (NAO, SST, ZW, and SLP) into the parametrization of the GEV models. Akaike Information Criterion (AIC) has been used to select the most appropriate probability function models. The methods of maximum likelihood were used for the estimation of the distributions parameters. The approach used considers the location ( $\mu$ ), the scale ( $\psi$ ), and the shape ( $\varepsilon$ ) parameters with relevant covariates, which are described by a selected climate index:

$$\mu(t) = \beta_{0,\mu} + \beta_{1,\mu}Y_1 + \dots + \beta_{n,\mu}Y_n, \quad (1)$$

$$\psi(t) = \beta_{0,\psi} + \beta_{1,\psi}Y_1 + \dots + \beta_{n,\psi}Y_n, \quad (2)$$

$$\varepsilon(t) = \beta_{0,\varepsilon} + \beta_{1,\varepsilon}Y_1 + \dots + \beta_{n,\varepsilon}Y_n, \quad (3)$$

where  $\beta_0, \beta_1, \dots, \beta_n$  are the coefficients, and  $Y_i$  is the covariate represented by the climate index. For each spectral component, only one climate index can be used among the parameters  $\mu$ ,  $\psi$ , and  $\varepsilon$  of the nonstationary GEV model. With the aim of optimizing the best use of the climate index into the different GEV parameters, a series of sensitivity analyses were implemented for each time scale. The AIC measures the goodness of fit of the model (Akaike, 1974) to the relation  $AIC = -2l + 2K$ ; where  $l$  is the log-likelihood value estimated for the fitted model, and  $K$  is the number of the model parameters. Higher ranked models should result from lower AIC scores.

## 3. Results

### 3.1. The multiscale sea-level variability

The variability of the total sea level (SL) and the surges (S) has been investigated using the continuous wavelet transform (CWT). In the spectrum of Fig. 3, the color scale represents an increasing power (variance) from blue to red. The CWT diagrams highlight the existence of several modes of variability; each color represents one of the energy bands with certain ranges of frequencies. The annual mode is clearly illustrated for SL while it is largely dissipated for S spectrum with a diminution higher than 90% in Dunkirk and Cherbourg. The dissipation of the annual spectrum becomes less important (with a spectrum diminution of 72%) for S in Le Havre as it gets closer to the Seine Bay, where the hydrological signature, induced by the Seine River, still remains to be observed within the stochastic component of the sea level.

At the interannual scales, the CWT diagrams highlight two modes of  $\sim 2$ –4-yr and  $\sim 5$ –8-yr at all the stations, particularly Cherbourg and Le Havre. Such low frequencies are well-structured with 45% and 65% of the explained variance higher than those calculated from the CWT of SL. The CWT diagrams of S display a new mode of  $\sim 1.5$ -yr while the annual mode, observed in the SL diagrams, has been disappeared.

The multiresolution analysis has been applied to local surges with the aim of achieving the full timescale decomposition of the signal. The process results in separation of different components or wavelet details for each signal (Figs. 4–6). We focused only on frequencies ranging between  $\sim 3$ -months and  $\sim 5$ –8-years, whose fluctuations correspond to the oscillation periods less than half the length of the record and exhibit a high-energy contribution on the variance of the total signal.

Results have been explored to investigate the dynamics of surges at different timescales. The variability is clearly dominated by the high-frequencies of  $\sim 3$ -months and  $\sim 6$ -months, explaining a variance between 35% and 45% of the total energy respectively (Table 1). Then, the low frequency components of  $\sim 1.5$ -yr,  $\sim 2$ –4-yr, and  $\sim 5$ –8-yr explain a mean variance of 25% of the total energy (Table 1).

Figs. 4–6 show a series of oscillatory components of surges from intermonthly to interannual scales, not clearly identified by a simple visual inspection of the signal. Similarities of surge components have been highly observed for the interannual modes of  $\sim 5$ –8-yr and  $\sim 2$ –4-yr while they seem to be significantly less important for high frequencies of  $\sim 3$ -months and  $\sim 6$ -months. This result suggests that different physical phenomena should be considered to explain the local variability of surges ( $\sim 3$ -months and  $\sim 6$ -months); they are induced by combining the effects of meteorological and oceanographic forces including changes in atmospheric pressures and wind velocities in shallow water areas. Beyond the  $\sim 1.5$ -yr timescale, the large-scale patterns of surges, described by the low frequency components, tend to be quite similar between the different sites in terms of intensity and amplitude. Such variability exhibits a global contribution of some physical processes related to the climate oscillations. The extent of these oscillations is not

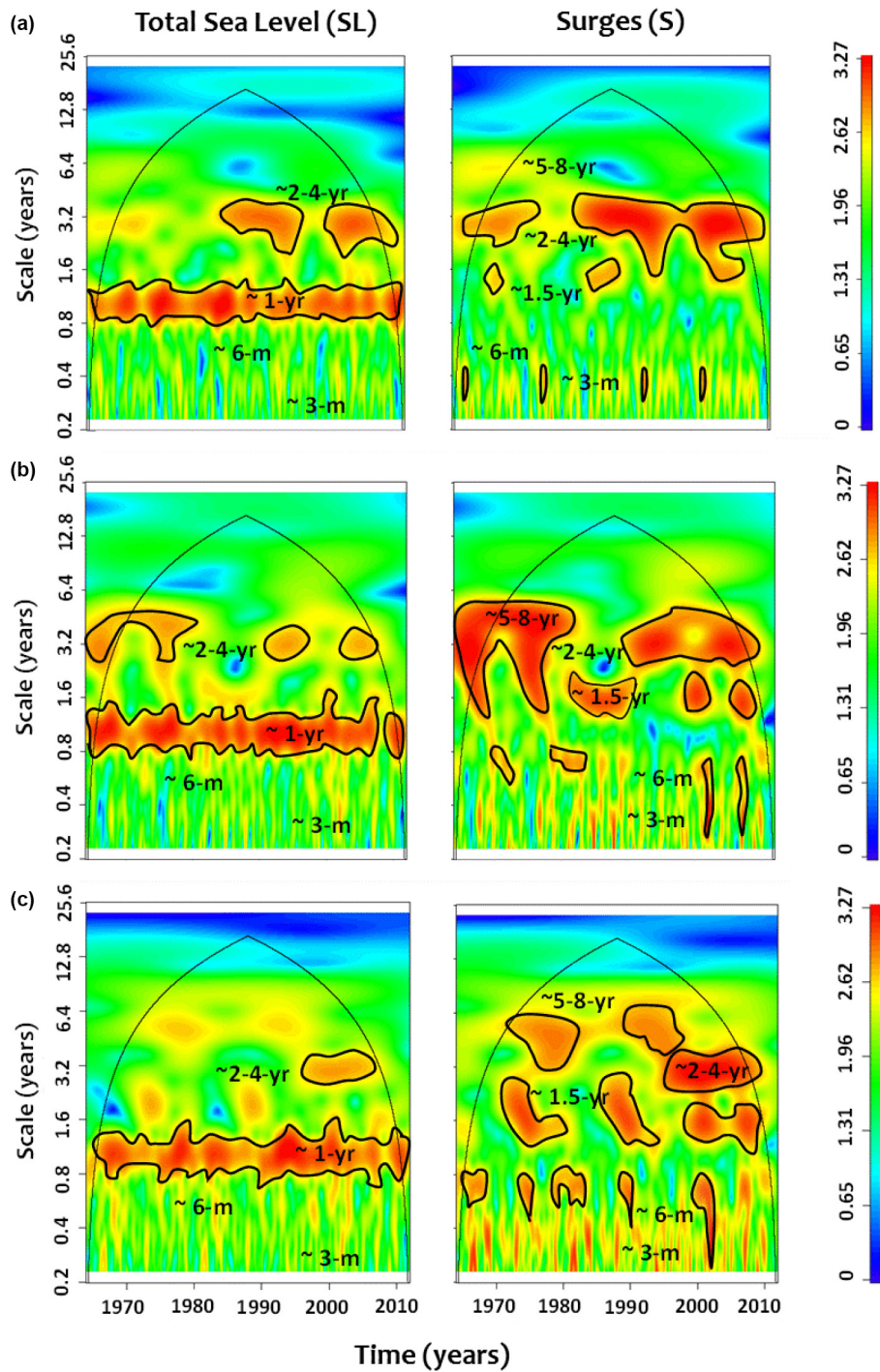


**Figure 3** Continuous wavelet transform (CWT) of the total and the non-tidal (surges) sea level at (a) Dunkirk, (b) Le Havre and (c) Cherbourg during the period 1964–2010.

**Table 1** The explained variance expressed as percentage of total variance of surges for all sites: Dunkirk, Le Havre and Cherbourg.

	~ 3 months	~ 6 months	~ 1.5- y	~ 2–4- y	~ 5–8-y
Dunkirk	20 %	15.6 %	12.8 %	8.6 %	5.3 %
Le Havre	27.7 %	18.2 %	14 %	8.8 %	5.7 %
Cherbourg	28.8 %	20.5 %	15.4 %	8.9 %	4.2 %

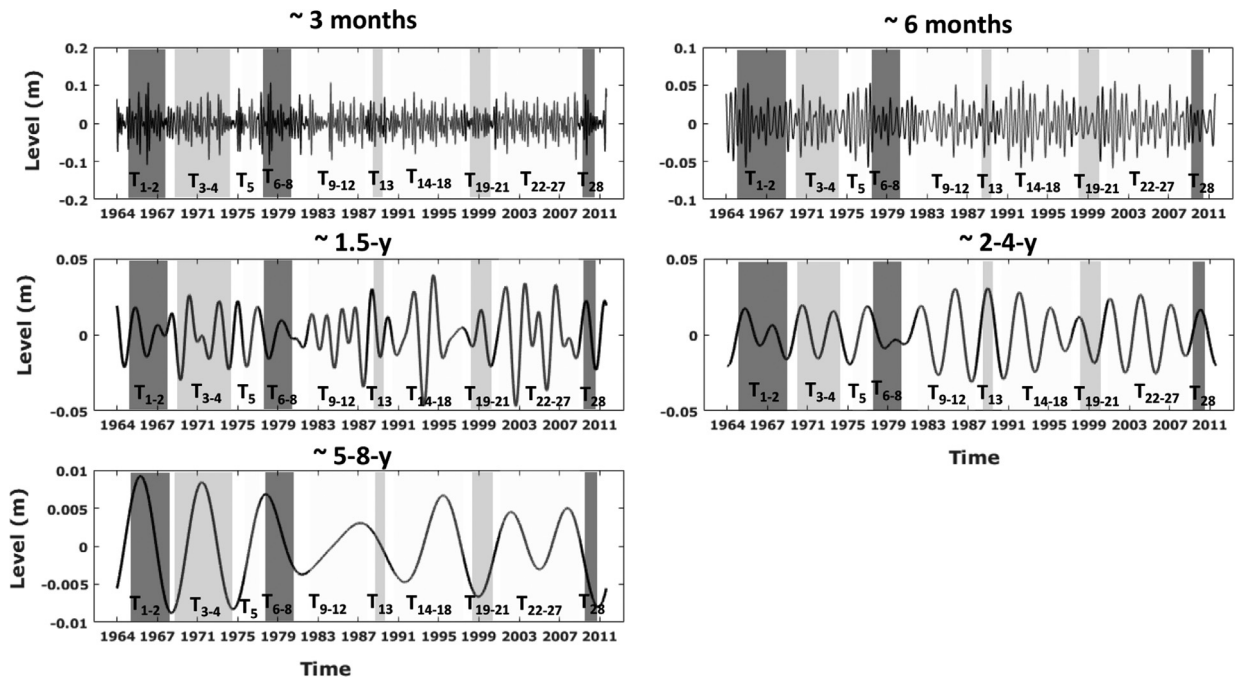


**Figure 4** Wavelet details (components) resulting from multiresolution analysis of surges from 1964 to 2012 at the intermonthly ( $\sim 3$  months,  $\sim 6$  months) and interannual ( $\sim 1.5$ -yr,  $\sim 2$ – $4$ -yr,  $\sim 5$ – $8$ -yr) time scales in Dunkirk. The black, grey and white boxes are used for storms manifested similarly in Le Havre and Cherbourg (same return period observed), similarly in Cherbourg and Dunkirk and similarly for all sites, respectively.

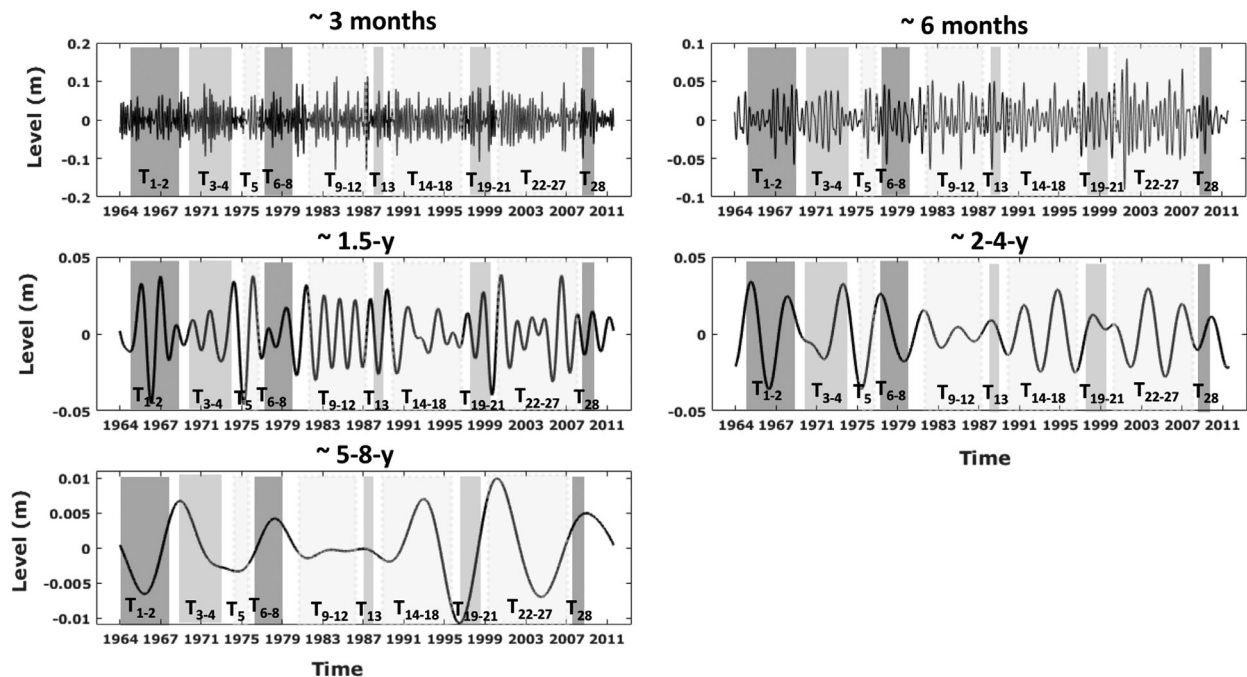


**Figure 5** Wavelet details (components) resulting from multiresolution analysis of surges from 1964 to 2012 at the intermonthly ( $\sim 3$  months,  $\sim 6$  months) and interannual ( $\sim 1.5$ -yr,  $\sim 2$ – $4$ -yr,  $\sim 5$ – $8$ -yr) time scales in Le Havre. The black, grey and white boxes are used for storms manifested similarly in Le Havre and Cherbourg (same return period observed), similarly in Cherbourg and Dunkirk and similarly for all sites, respectively.

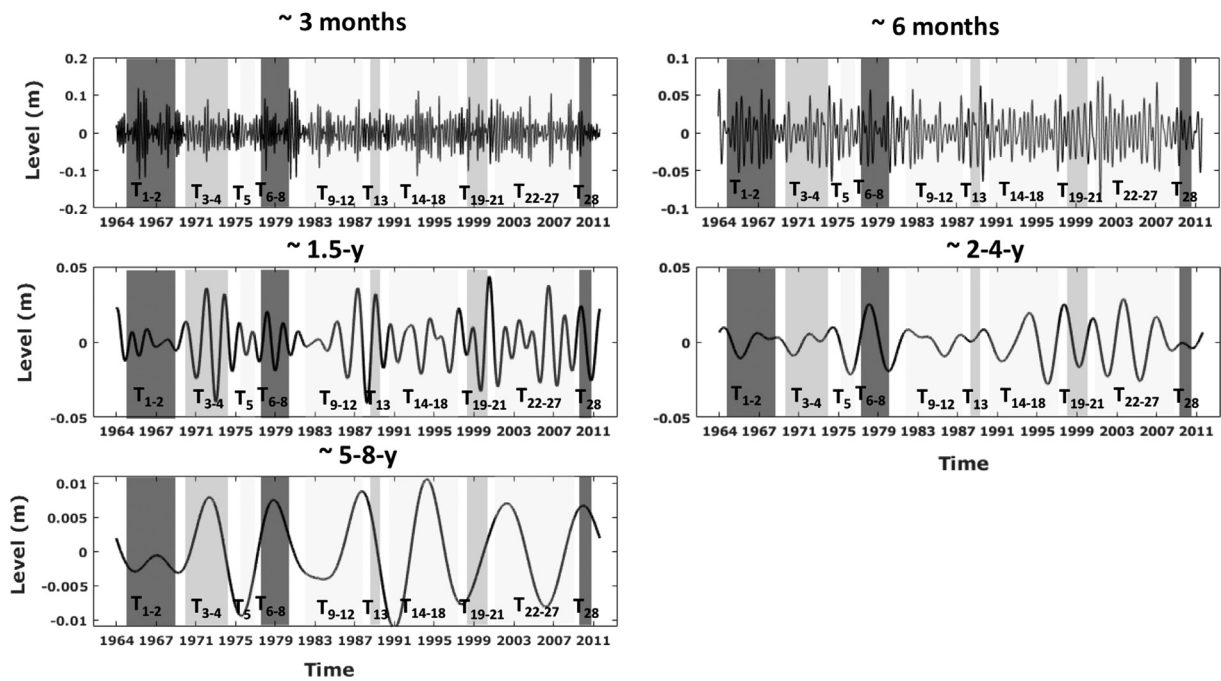


**Figure 6** Wavelet details (components) resulting from multiresolution analysis of surges from 1964 to 2012 at the intermonthly ( $\sim 3$  months,  $\sim 6$  months) and interannual ( $\sim 1.5$ -yr,  $\sim 2$ – $4$ -yr,  $\sim 5$ – $8$ -yr) time scales in Cherbourg. The black, grey and white boxes are used for storms manifested similarly in Le Havre and Cherbourg (same return period observed), similarly in Cherbourg and Dunkirk and similarly for all sites, respectively.

strictly similar and changes according to the timescale variability since the dynamics of surges is not necessarily related to the same type of atmospheric circulation process. This relationship will be addressed later in the second part of this section.

A total of 28 historical stormy events (from  $T_1$  to  $T_{28}$ ), produced in the English Channel during the period 1964–2010 and with surges higher than 2-yr return period level ( $Re$ ), have been extracted from SHOM data base (Table 2). The historical events have been attached to the different spectral components of surges (Figs. 4–6) by vertical bars with different colors (black, grey and white).

In these figures, we distinguish three types of events: (1) the first one, depicted by the black bars, represents the storms occurring in Le Havre and Cherbourg with the same  $Re$ ; (2) the second one, depicted by the white bars, shows the storms similarly manifested in Cherbourg, Le Havre and Dunkirk; (3) the third one, depicted by the grey bars, illustrates the storms occurring in Le Havre and Cherbourg with the same  $Re$ . The percentages of each of the bars are 21.4, 57.2, and 21.4%, respectively.

The storms in Figs. 4–6 show that the signature of each event is fully identified at the intermonthly scales while it is manifested differently at the interannual scales.

The events of November 1965 ( $T_1$ ) and January 1968 ( $T_2$ ), produced at neap tides, are highlighted by the peak of the surges at the interannual scales; they are limited to  $\sim 1.5$ -yr and  $\sim 2$ – $4$ -yr in Le Havre and Cherbourg where  $Re$  is of 2–5 years. The storms  $T_3$  (July 1969) and  $T_4$  (February 1974) exhibit a high energy for most of the components in Le Havre ( $Re$  of 5–10 years), as shown in Fig. 5; furthermore, their effects are limited to  $\sim 1.5$ -yr component in Dunkirk and

Cherbourg. As documented by Bessemoulin (2002), these storms (in particular  $T_3$ ) were resulted from the big atmospheric depression Ex-Bertha with high wind velocities (more than 150 km/h) and barometric gradients (maximum of 14 hPa).  $T_5$  is manifested in different locations with  $Re$  of 2-years; its impact is restricted to the  $\sim 1.5$ -yr component of surges. Similar behavior has been identified for the events  $T_9$ – $T_{12}$ ,  $T_{15}$ – $T_{16}$ , and  $T_{18}$  produced at neap tides. The events  $T_6$  (January 1978),  $T_{13}$  (February 1989), and  $T_{14}$  (January 1990, ‘DARIA’) coincide with spring tides and high return period ( $Re > 5$  years); they have been recorded at the interannual scales in Le Havre and Cherbourg. According to the previous works of Bessemoulin (2002) and Pirazzoli et al. (2005), these events were induced by cold fronts known as Kata split front responsible for decreasing of the pressure and a shift of the wind from SSW to WSW.

The events  $T_7$ ,  $T_8$ , and  $T_{17}$  were produced during winter periods at the equinoxes of spring tides with  $Re$  of 5–10 years; they are manifested at the full interannual timescales (from  $\sim 1.5$ -yr to  $\sim 5$ – $8$ -yr) in Le Havre and Cherbourg. Such events were generated by two huge anticyclones with large pressure gradients from the North to the West: the first one was resulting from the NW winds; the second one was coming from the Atlantic to reach the North Sea and the Scandinavian countries, responsible for more than 70% of the submersion phenomena in the NW France (Costa et al., 2004).

The two storms of  $T_{19}$  (December 1999) and  $T_{20}$  (December 2001) highlighted a clear signature limited to  $\sim 1.5$ -yr in Dunkirk and Cherbourg while they are manifested at different interannual scales than Le Havre, close to the Seine Bay, where the influence of the hydrological variability is

**Table 2** List of storminess with a surge return period (Re) higher than 2 years and produced between 1964 and 2010 in Dunkirk, Le Havre, and Cherbourg. The black, grey, and white boxes are used for storms manifested similarly in Le Havre and Cherbourg (same return period observed), similarly in Cherbourg and Dunkirk and similarly for all sites, respectively.

Code	Date	Surge return period	Tide cycle
T <sub>1</sub>	November, 1965	H <sub>5</sub> –H <sub>10</sub> (Dunkirk) H <sub>2</sub> –H <sub>5</sub> (Le Havre, Cherbourg)	Neap tide
T <sub>2</sub>	January, 1968	H <sub>5</sub> –H <sub>10</sub> (Dunkirk) H <sub>2</sub> –H <sub>5</sub> (Le Havre, Cherbourg)	Neap tide
T <sub>3</sub>	July, 1969	H <sub>2</sub> (Dunkirk, Cherbourg) H <sub>5</sub> –H <sub>10</sub> (Le Havre)	Neap tide
T <sub>4</sub>	February, 1974	H <sub>2</sub> (Dunkirk, Cherbourg) H <sub>2</sub> –H <sub>5</sub> (Le Havre)	Spring tide
T <sub>5</sub>	December, 1976	H <sub>2</sub> (Dunkirk, Le Havre, Cherbourg)	Neap tide
T <sub>6</sub>	January, 1978	H <sub>5</sub> –H <sub>10</sub> (Dunkirk) H <sub>5</sub> (Le Havre, Cherbourg)	Spring tide (equinoxes)
T <sub>7</sub>	December, 1979	H <sub>5</sub> –H <sub>10</sub> (Le Havre, Cherbourg) H <sub>5</sub> (Dunkirk)	Spring tide (equinoxes)
T <sub>8</sub>	December, 1981	H <sub>5</sub> –H <sub>10</sub> (Le Havre, Cherbourg) H <sub>5</sub> (Dunkirk)	Spring tide
T <sub>9</sub>	December, 1982	H <sub>2</sub> (Dunkirk, Le Havre, Cherbourg)	Neap tide
T <sub>10</sub>	January, 1984	H <sub>2</sub> (Dunkirk, Le Havre, Cherbourg)	Neap tide
T <sub>11</sub>	March, 1986	H <sub>2</sub> (Dunkirk, Le Havre, Cherbourg)	Neap tide
T <sub>12</sub>	October, 1987	H <sub>2</sub> (Dunkirk, Le Havre, Cherbourg)	Neap tide
T <sub>13</sub>	February, 1989	H <sub>5</sub> –H <sub>10</sub> (Cherbourg, Dunkirk) H <sub>2</sub> –H <sub>5</sub> (Le Havre)	Spring tide
T <sub>14</sub>	January, 1990 (DARIA)	H <sub>5</sub> –H <sub>10</sub> (Dunkirk, Le Havre, Cherbourg)	Neap tide
T <sub>15</sub>	May, 1992	H <sub>2</sub> (Dunkirk, Le Havre, Cherbourg)	Neap tide
T <sub>16</sub>	September, 1993	H <sub>2</sub> (Dunkirk, Le Havre, Cherbourg)	
T <sub>17</sub>	December, 1995	H <sub>5</sub> –H <sub>10</sub> (Dunkirk, Le Havre, Cherbourg)	Spring tide (equinoxes)
T <sub>18</sub>	October, 1998	H <sub>2</sub> (Dunkirk, Le Havre, Cherbourg)	Neap tide
T <sub>19</sub>	December, 1999	H <sub>2</sub> (Dunkirk, Cherbourg) H <sub>5</sub> –H <sub>10</sub> (Le Havre)	Spring tide
T <sub>20</sub>	December, 2001	H <sub>2</sub> (Dunkirk, Cherbourg)	Spring tide
T <sub>21</sub>	February, 2004	H <sub>5</sub> –H <sub>10</sub> (Le Havre) H <sub>5</sub> –H <sub>10</sub> (Dunkirk, Cherbourg) H <sub>5</sub> (Le Havre)	Neap tide
T <sub>22</sub>	April, 2005	H <sub>2</sub> –H <sub>5</sub> (Dunkirk, Le Havre, Cherbourg)	Spring tide
T <sub>23</sub>	March, 2006	H <sub>2</sub> –H <sub>5</sub> (Dunkirk, Le Havre, Cherbourg)	Spring tide (equinoxes)
T <sub>24</sub>	November, 2007	H <sub>2</sub> (Dunkirk, Le Havre, Cherbourg)	Neap tide
T <sub>25</sub>	March, 2008	H <sub>5</sub> –H <sub>10</sub> (Dunkirk, Le Havre, Cherbourg)	Spring tide (equinoxes)
T <sub>26</sub>	January, 2009	H <sub>2</sub> –H <sub>5</sub> (Dunkirk, Le Havre, Cherbourg)	Neap tide
T <sub>27</sub>	February, 2010	H <sub>5</sub> –H <sub>10</sub> (Dunkirk, Le Havre, Cherbourg)	Spring tide
T <sub>28</sub>	December, 2010	H <sub>2</sub> –H <sub>5</sub> (Dunkirk) H <sub>5</sub> –H <sub>10</sub> (Le Havre, Cherbourg)	Neap tide

important during the flooding events between 20th century and the beginning of 21<sup>st</sup> century (Massei et al., 2017).

$T_{21}$  (February 2004) was produced at neap tides with strong winds of 140 km/h (SHOM, 2014); this event is mainly carried out by the interannual components.  $T_{22}$  and  $T_{23}$  (Re between 2 and 5 years), were recorded for the sites at the scales of  $\sim 1.5$ -yr and  $\sim 2$ –4-yr while  $T_{24}$  (Re of 2 years) is limited to  $\sim 1.5$ -yr. The last events  $T_{25}$ ,  $T_{27}$ , and  $T_{28}$  (Re > 5 years) occurred during the winter periods the equinoxes of spring tides, are manifested at all timescales in Le Havre and Cherbourg and seem to be limited to  $\sim 4$ –8-yr component in Dunkirk.

Accordingly, the multiscale variability of the surges, as a response to extreme events, highlights that 14% of storms are manifested at all the interannual timescales while 32% of them are limited to  $\sim 2$ –4-yr. This correspondence suggests the relationship between the return period of the storms and the multiscale variability of the surges; storms with Re < 5 years are manifested at timescales smaller than 5 years while storms with high Re of 5–10 years should be observed from the intermonthly to the interannual scales of  $\sim 5$ –8-yr.

This diagnosis of the historical events and their manifestation along the North French coasts (From Dunkirk to Cherbourg) allows the following classification: (i) the events produced at neap tides and similarly affecting the studied sites of the Normandy coasts at the interannual scales of  $\sim 1.5$ -yr ( $T_5$ ,  $T_{9-12}$ ,  $T_{15-16}$ , and  $T_{18}$ ) and  $\sim 2$ –4-yr ( $T_{22}$  and  $T_{23}$ ); (ii) the events induced by Kata split font under spring tides and evolving similarly in Le Havre and Cherbourg and with higher impact in Dunkirk ( $T_6$  and  $T_{13-14}$ ); (iii) the events induced by a combination of two anticyclones effects, from the Atlantic to the North Sea, and affecting similarly Le Havre and Cherbourg and with a less remarkable impact in Dunkirk ( $T_{17}$  and  $T_{7-8}$ ); (vi) the events produced at spring tides and highly affecting Le Havre at different timescales compared to Dunkirk and Cherbourg where their manifestation is limited to  $\sim 1.5$ -yr ( $T_{3-4}$  and  $T_{19-21}$ ).

The distribution of the storms is not homogenous in time; moreover, their manifestation, according to different categories of return period, takes a nonlinear behavior since the number of the events in a window of one year is not the same throughout the time. Indeed, all significant events (Re > 2 years) have been identified during only 20 years of measurements from 46 years, the total period of the present study (1964–2010). These dynamics explain the altering phases of high (Re > 2 years) and moderate (Re < 2 years) storms in accordance with their return period. Moderate phases are longer with 3–4 successive years during the first 35 years (1964–2000) and decrease to 2 years after 2000. The phases of high storms exhibit different categories of events: 75% of them are produced between November and February and 25% of them are produced between March and October.

Hence, the distribution of storminess is controlled by a series of seasonal patterns related to changes in ocean wave climate and energy conditions. These seasonal oscillations are clearly identified at the intermonthly surges ( $\sim 3$ –6-months) for all sites. At this scale, similar oscillations have been demonstrated by Tsimplis and Woodworth (1994) from the analysis of the mean sea levels. According to the obtained results, the stormy events, produced under specific

meteorological and oceanographic conditions on tides, have exhibited a strong seasonal dependence on the tides which underline a complex network induced by a nonlinear contribution of many physical processes. The hydrological effect should be also considered in the present context of the Seine Bay where the river discharge contributes in the total variability of the stochastic component, in particular during the extreme events of the flooding produced between 1999 and 2001.

Haigh et al. (2010) used English Channel sea-level dataset from 18 tide gauges to evaluate the changes in the extremes throughout the 20<sup>th</sup> century. They have identified different intra- and inter-decadal variability in surges with the strongest intensity on the late 1950s. Their studies have shown strong relationship between the storm surges and the NAO index with weak negative correlations throughout the Channel and strong positive correlations at the boundary along the Southern North Sea. The interactions of tides with surges have also been investigated by the same authors showing their increase eastward along the English Channel. The tide-surge interaction has been also studied by Idier et al. (2012) using a numerical approach to compute some historical storms in the Atlantic and the North Sea. According to their analyses, the tide-surge interaction in the English Channel is significantly important; it increases in the eastern half of the English Channel and decreases in westerly direction. In the present research, the stochastic signal of surges has been individually studied and its interaction with tides has not taken into account. The neap-spring tidal cycle has been considered to investigate the dynamics of the stormy events along the French coasts and their signatures in different intermonthly and interannual components of the extreme surges.

### 3.2. How does the variability in extreme surges depend on the global atmospheric circulation?

This part focuses on the connection between the multiscale variability of the local surges along the French coasts and the global climate oscillations.

The monthly extrema have been simulated from the hourly records of surges in the considered sites. The monthly distribution of the extreme values has been calculated for each scale from the intermonthly to the interannual modes and illustrated by the means of boxplot presentations (example for Dunkirk in Fig. 7). These distributions exhibit that the maximum surges change according to the timescale; the multiscale evolution shows an oscillatory behavior for the short-scales (intermonthly and the first interannual of  $\sim 1.5$ -yr) shifting between high and low changes in April and September. This shift is more visible at the intermonthly scales of  $\sim 3$ -months and  $\sim 6$ -months. For larger scales, the extreme surges display a uniform evolution during the time.

With the aim of addressing the nonstationary behavior of the extreme surges, we have applied the wavelet multiresolution decomposition of monthly extrema for each site. The process has resulted in the separation of different components, i.e. 5 wavelet details traduced by two intermonthly scales ( $\sim 3$ -months and  $\sim 6$ -months) and three interannual scales ( $\sim 1.5$ -yr,  $\sim 2$ –4-yr, and  $\sim 5$ –8-yr). The explained

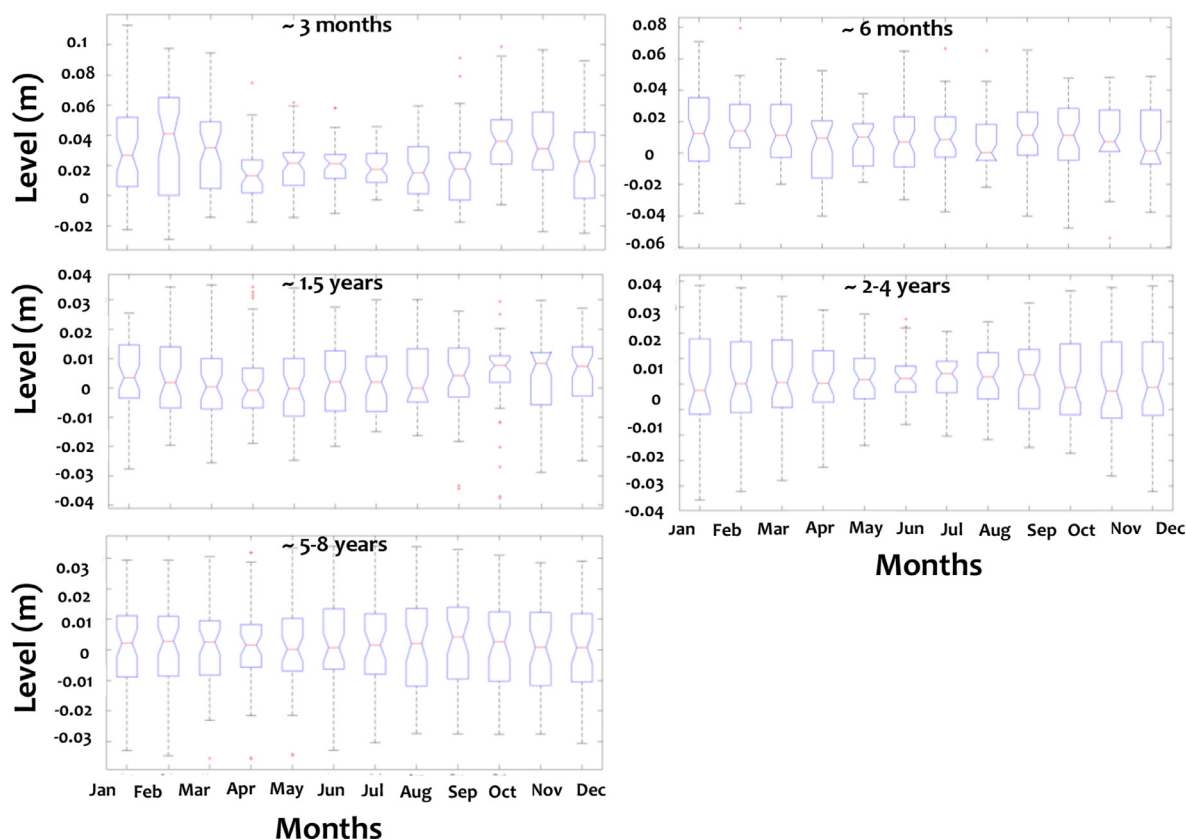


**Figure 7** The boxplot of the monthly maxima of surges on the intermonthly ( $\sim 3$  months and  $\sim 6$  months) to the interannual ( $\sim 1.5$ -yr;  $\sim 2$ – $4$ -yr and  $\sim 5$ – $8$ -yr) scales; case of Dunkirk.

variances of these scales are higher than those resulting from the multiresolution analysis of the hourly surges: the variance of the intermonthly scales has a mean percentage of 45% of the total signal while the interannual scales vary between 28% and 36%.

Then, the nonstationary behavior of the monthly extreme surges has been addressed by investigating their physical connections with the different climate indices (i.e. SST, SLP, ZW, and NAO). The total signal (not decomposed) of the climate indices has been linked to the extreme components calculated previously. For each spectral component, a series of Monte Carlo simulations have been carried out to identify the most statistically significant correlation with the climate index. The best correlation of each surge component (i.e.  $\sim 3$ -months and  $\sim 6$ -months,  $\sim 1.5$ -yr,  $\sim 2$ – $4$ -yr and  $5$ – $8$ -yr) with the suitable climate index (i.e. SST, SLP, ZW, and NAO) is illustrated in Fig. 8. The correlation coefficients vary between 0.5 and 0.6 at the intermonthly scales (i.e.  $\sim 3$ -months and  $\sim 6$ -months) showing good agreements of SST index with the extreme surges. The  $\sim 1.5$ -yr component is linked to SLP index with correlation coefficients varying between 0.65 and 0.7. Significant coefficients higher than 0.7 have been observed for the interannual scales of  $\sim 2$ – $4$ -yr and  $\sim 5$ – $8$ -yr exhibiting strong links with ZW and NAO indices respectively.

In the second part of this section, a stationary and a nonstationary extreme value analyses based on the GEV distribution with time-dependent parameters (Coles, 2001) have

been implemented to model the spectral component of the monthly maxima of the surges.

Here, we are interested to separately model the different components of the extreme surges by using the GEV distribution. The GEV distribution uses the maximum likelihood method with a parametrization of the different parameters of location, scale, and shape.

Five stationary GEV models (GEV01, GEV02, GEV3, GEV04, and GEV05) have been used to fit the different spectral components of the monthly extreme surges. The AIC criterion has been calculated for each spectral component (Table 3) to compare their distributions. Results show higher AIC scores for the intermonthly scales of  $\sim 3$ -months and  $\sim 6$ -months (GEV01 and GEV02); they decrease at larger-scales of  $\sim 5.8$ -yr (GEV05). The differences between the observed extreme values and the empirical ones, calculated from the stationary GEV models (from GEV01 to GEV05), should be explained by significant discrepancies which vary according to the timescale of the extreme surges. These discrepancies decrease in the sites where the interannual scales (i.e. GEV04 and GEV05) experience a uniform trend of extremes.

With the aim of improving the modelling of extreme surges, five nonstationary GEV models (GEV1, GEV2, GEV3, GEV4 and GEV5) have been applied to all spectral components. The parameters of the nonstationary GEV distribution have been estimated using the maximum likelihood method (Coles, 2001). Maximizing the log-likelihood function has

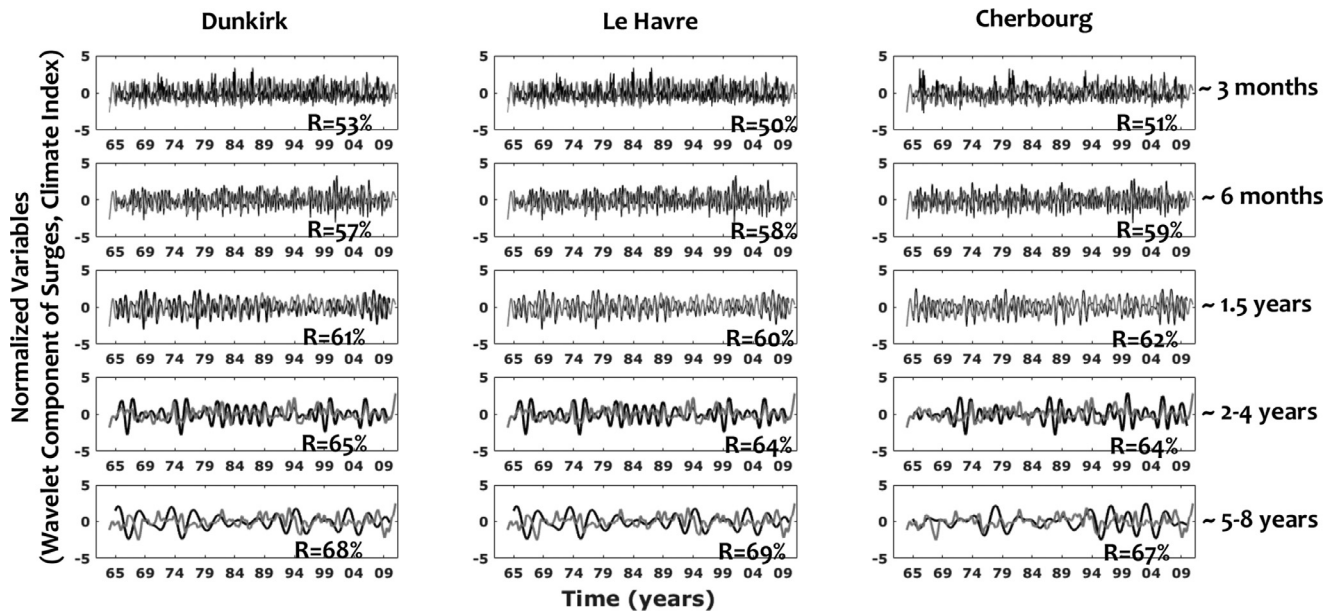


**Figure 8** Multiresolution decomposition of the monthly maxima of surges (black line). The signal of climate oscillations associated with the different indices SST, SLP, ZW, NAO (grey line) has been correlated to the spectral components of surges. Only the connection maximizing the correlation coefficient between a selected climate index and the component of surges (from intermonthly to interannual timescales) is presented (the normalized values have been calculated to superpose both signals). The correlation coefficients are also displayed at each time scale.

**Table 3** Akaike Information Criterion (AIC) test results for distribution models of extreme surges using the stationary GEV model.

	~ 3 months	~ 6 months	~ 1.5- y	~ 2–4 –y	~ 5–8-y
Dunkirk	-450	-352	-324	-352	-345
Le Havre	-410	-322	-320	-350	-352
Cherbourg	-395	-301	-314	-345	-350

**Table 4** Akaike Information Criterion (AIC) test results for the distribution models of the extreme surges using the nonstationary GEV model.

	~ 3 months/SST	~ 6 months/SST	~ 1.5- y/SLP	~ 2–4 –y/ZW	~ 5–8-y/NAO
Dunkirk	-310	-282	-266	-248	-232
Le Havre	-308	-279	-260	-252	-243
Cherbourg	-315	-285	-264	-245	-245

been performed by means of the ‘trust region reflective algorithm’ (Coleman and Li, 1996).

For each model, the best climate index describing the internal oscillations of the monthly maxima has been used as a covariable in GEV distribution to address the nonstationary behavior of the extreme values. For each spectral component, the structure of the most appropriate nonstationary GEV distribution has been selected by choosing the most adequate climate index that minimizes the Akaike information criterion (Akaike, 1974). Here, the total signal of the climate index has been used as shown in Fig. 8. The goodness of the fit of each model has been checked through the visual inspection of the quantile-quantile (Q-Q) plots; these plots compare the empirical quantiles against the quantiles of the fitted model. The substantial departure from the diagonal indicates an inadequacy of the GEV model.

Results provided by GEV1–5 reveal a better performance (the lowest values of AIC) of extreme estimation compared to the previous models of GEV01–05 and give the most appropriate distributions by the use of the climate oscillations. Indeed, the SLP, ZW, and NAO indices have been used for the interannual scales of ~1.5-yr, ~2–4-yr, and ~5–8-yr respectively while the SST index has been selected as the most adequate for the intermonthly scales of ~3-months and ~6-months (Table 4). The Q-Q plots for the all timescales of the monthly maxima in Dunkirk are illustrated in Fig. 9; they confirm the suitability of the selected models.

Accordingly, the nonstationary GEV models have exhibited high improvements at all timescales, in particular at the intermonthly scales (GEV01/GEV1; GEV02/GEV2) where the AIC scores have significantly decreased.

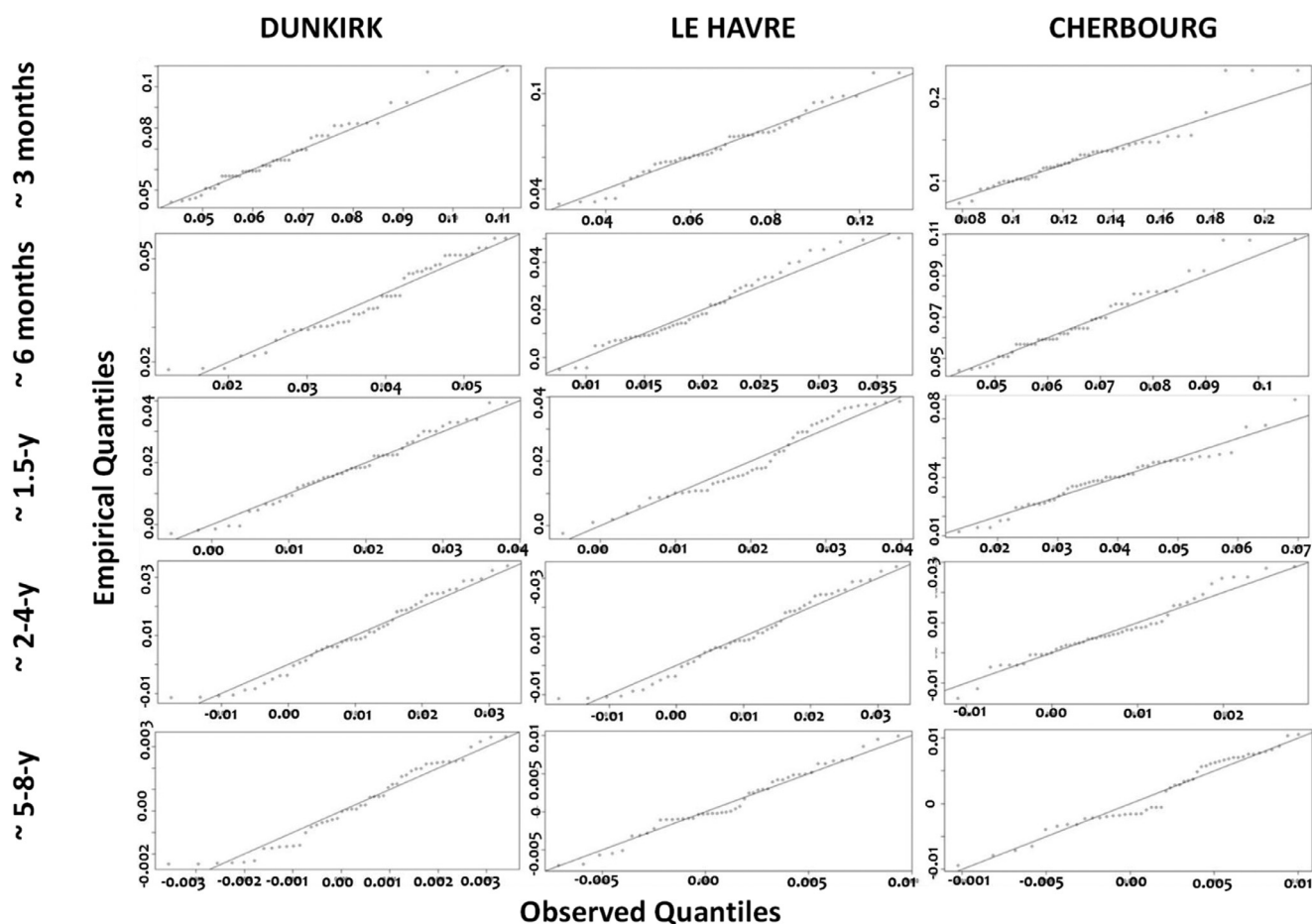


**Figure 9** The quantile plot between observed and modelled extreme surges obtained using the nonstationary GEV model at different time scales.

#### 4. Discussion

Results provided in the present research highlight the origin of the nonlinear relationship between large- and local-scales. Indeed, the intermonthly and the interannual extreme surges may be related to different combinations of several, not necessarily similar, oscillating atmospheric patterns. The use of a multiresolution approach to investigate the dynamics of the extreme surges into the downscaling studies proves to be useful for assessing the nonlinear interactions between large-scale climate variability and local-scale hydrodynamic changes of the sea-level hydrodynamics.

Investigating the physical relationships of the climate oscillations with the multiscale surges have shown that the multimodel climate ensemble should be used to better understand this complexity, in particular for extreme events.

The seasonal and the interannual physical relationships between the local hydrodynamics and the climate variability have been investigated in numerous previous works. They focused on the atmospheric circulation with different related mechanisms (e.g., Feliks et al., 2011; Lopez-Parages et al. 2012; Zampieri et al., 2017).

The use of the SST index to estimate the intermonthly extreme surges shows that their seasonal variability should be related to the variation of temperature in the sea surface

controlled by an important atmosphere-ocean interaction in the Atlantic Sea. For short-scales, Bell and Goring (1998) investigated the relationship between the seasonal variations of the sea level and the SST along the north-east coasts of the New Zealand. They have demonstrated that the dominant influence of SST on the annual cycle of sea level is related to the thermo-steric sea-level adjustments with 50–80% of the variance in the annual frequency. Their works have suggested that the sea level generally peaks at the end of April (austral autumn) lagging the SST cycle by around 2 months, and its seasonal modulation is explained by changes in the oceanic current patterns and the seasonal coupling of climate oscillation effects. Previous studies have indicated the impact of the midlatitude SST gradients on the atmospheric circulation influencing the amplitude and the location of the storm tracks (e.g., Nakamura and Yamane 2009; O'Reilly and Czaja 2015; Small et al., 2014). For large-scales, the key role of SST in the atmosphere-ocean interaction has been also addressed by several works. According to some observational studies, the meridional shifts in the location of the Gulf Stream extension fronts are significantly linked to the large-scale variations in the atmospheric circulation at the intraseasonal timescales (e.g., Frankignoul et al., 2011). Recently, Wills et al. (2016) have examined the atmosphere-ocean interaction over the Gulf Stream and its relation with two potential different patterns of atmospheric circulation

anomalies: one pattern leads to SST field and another resultant pattern lags the SST field and is considered as an atmospheric response to midlatitude ocean forcing (Wills et al., 2016).

The spatial distribution of the SST anomalies is strongly related to the study area, the influence of the seabed topography and the runoff conditions. Considering the cases of the Bristol Channel (Mayes and Wheeler, 2013) and the Seine Bay in the English Channel, negative anomalies of SST are generally located near to coastal zones connected to hydrological systems and influenced by rivers and the annual regime of precipitations. The Northern Atlantic SST fields have been hypothesized to be linked to the interannual and the decadal persistence of atmospheric circulation anomalies (Namias, 1969; 1972). These anomalies have been defined to be connected to the Atlantic Multidecadal Oscillation (AMO) as a natural mode of variability (e.g., Schlesinger and Ramankutty, 1994).

Lopez-Parages et al. (2012) have studied the statistical predictability of the rainfall variability and stated that it can be improved by selecting the most suitable predictors depending on the period on which the prediction is carried out. They have also suggested that the nonstationary link of the rainfall with SST takes place when the dipolar patterns of the rainfall are reinforced with the negative phases of the AMO (Atlantic Multidecadal Oscillation) along the 20<sup>th</sup> century. In this study, the seasonal modulations of surges have displayed strong links with changes in SST phases. The SST patterns, due to the intrinsic modes of the atmospheric circulation variability, play a key role in regulating the global climate change and thus providing a source of potential predictability for the climate fluctuations on seasonal timescales. For larger scales, the SST index can be related to the Atlantic Multidecadal Oscillation.

The correlation between the  $\sim 1.5$ -yr interannual variability of extreme surges and the SLP index has been demonstrated for the study sites in this work. In this context, Turki et al. (2019) investigated the connection between the local dynamics of the surges and the global atmospheric circulation from SLP composites. They have suggested dipolar patterns of high-low pressures with a series of anomalies at the interannual and the interdecadal scales which should be related to the physical mechanisms linked to the North-Atlantic and ocean/atmospheric circulation oscillating at the same timescales. As documented by Frankignoul et al. (2011), the SLP fields and the baroclinic instability of wind stress are related to the Gulf Stream path as given by NCEP reanalysis; the dominant signal is a northward (southward) displacement of the Gulf Stream when the NAO reaches positive (negative) extrema. Zampieri et al. (2017) used the daily mean SLP fields to analyze the influence of the Atlantic sea temperature variability on the day-by-day sequence of large-scale atmospheric circulation patterns over the Euro-Atlantic region. They have found significant changes in the frequencies of certain weather regimes associated with the phase shifts of the AMO. For hydrological applications, several works have investigated the multiscale relationships between the local hydrological changes and the climate variability. Lavers et al. (2010) associated the 7.2-yr timescales to SLP patterns which are not exactly reminiscent of the NAO and define centers of action which are shifted to the North.

The relationship between the ZW index and the  $\sim 2$ -4-yr interannual variability of extreme surges has been significantly validated for the different sites of the English Channel coasts (as shown by GEV4). The ZW is generally associated with the atmospheric jets induced by the geostrophic equilibrium with the zonal mean height gradients. The wind-stress anomalies induce a zonal wind-stress increasing over the subtropical and the subpolar gyre boundaries. The fast barotropic response to the wind stress is explained by easterly winds in the Tropics and westerly winds in the mid-latitude (Wang, 2001). According to some previous works (e.g., L'Heureux and Thompson 2006; Seager et al. 2003), the inter-hemispheric symmetry of both temperature and zonal wind bears great resemblance to regression patterns associated with the observed El Niño. Lu et al. (2008) investigated El Niño minus La Niña composites for the air temperature, zonal wind, and the tropopause pressure level. They derived these parameters from the difference of patterns between 14 warm years and 12 cold years. They have demonstrated that the tropospheric zonal wind is intensified near the equatorward flank of the jet, resulting in a equatorward strengthening of the jet. Andrade et al. (2012) investigated the extreme temperature in Europe and its occurrence in relation to the large-scale atmospheric circulation. They used the zonal wind component at 850 hPa to identify the positive and negative phases of the extreme periods. They suggested that both phases of extreme temperature changes are commonly connected to strong large-scale changes in zonal and meridional transports of heat and moisture, resulting in changes in the temperature patterns over western and central Europe (Corte-Real et al., 1995; Trigo et al., 2002). The studies from Mizuta (2012) and Zappa et al (2013) have demonstrated the physical links between the ZW and the extreme events from 11 Global Climate Model runs, suggesting the complex relationship between the climate oscillation and the jet stream activity. They have found a slight increase in the frequency and strength of the storms over the central Europe and decreases in the number of the storms over the Norwegian and Mediterranean seas.

In the English Channel and along the UK and the Northern coasts, changes in trends of the extreme waters and storm surges have been explained by the variations of the energy pressure and ZW variability additional to the thermodynamic fluctuations. These studies are in closer agreements with the present research where strong physical links between the ZW and the interannual component  $\sim 2$ -4-yr of the extreme surges have been demonstrated along the English Channel coasts (North France)

In the present study, the larger scales of the  $\sim 5$ -8-yr extreme surges have been linked to the NAO index. In agreement with other previous works (e.g. Marcos et al., 2012; Philips et al., 2013), the NAO is considered as an influencing climate driver for the large-scale atmospheric circulation. The physical mechanisms explaining the effects of the continuous changes in NAO patterns on the sea-level variability have been addressed in several studies (e.g., Trisimplitis and Josey, 2001). Investigating the low frequencies of the sea levels has shown the existence of the long-term oscillations that originate from large-scale climate variability and thus control the interannual extreme surges along the English Channel. The key role of the NAO on the interannual

sea-level variability has been explained by some previous works: Philips et al. (2013) investigated the influence of the NAO on the mean and the maximum extreme sea levels in the Bristol Channel/Severn Estuary. They have demonstrated that when high NAO winters increase in the positive phase, wind speeds also escalate while increasing the negative NAO winters results in low wind speeds. Then, the correlation between the low/high extreme surges and the NAO in the Atlantic has demonstrated a proportionality between NAO values and the augmentation in the winter storms. Feliks et al. (2011) defined significant oscillatory modes periods of ~2.8-yr, ~4.2-yr, and ~5.8-yr in both observed NAO index and NAO atmospheric marine boundary layer simulations forced with SST; they have suggested that the atmospheric oscillatory modes should be induced by the Gulf Stream oceanic front.

We can conclude that different atmospheric oscillations could be related to the variations in the extreme surges according to the timescale considered; for each scale, its best physical connection with a specific climate oscillation is proven. This result suggests that the atmospheric circulation acts as a regulator controlling the multiscale variability of extreme surges with a nonlinear connection between the large-scale atmospheric circulation and the local scale hydrodynamics. Such nonlinear characteristics depend on the dynamics of the different sequences of the atmospheric and water vapour transport patterns during the month prior to the sea-level observations (e.g., Lavers et al., 2015).

The multiscale dependence of the local-scale hydrodynamic changes on the internal modes of the global-scale climate oscillations is still under debate. The use of the diverse indices of SST, NAO, ZW, and SLP could improve the estimation of the extreme values in the oceanography tasks and deepen the scientific understanding of the physical dynamics of surges in coastal environments.

In this work, the signal of surges has been linearly extracted from the total sea level time-series by the use of the classical harmonic analysis and thanks to the assumption that the water level is the sum of the mean sea level, tides, and surges. This assumption is not completely valid in the English Channel where the significant tide-surge interactions (Tomassin & Pirazzoli, 2008) and the effects of the sea-level rise on tides and surges are important (e.g. Idier et al., 2017).

Neglecting this nonlinear interaction between the surges, tides, and the sea-level rise in the present work suggests some uncertainties in the estimation of the spectral components from the instantaneous and monthly extreme surges. These uncertainties, extracted from the multiresolution analysis of, could not affect the main results of the present work since the nonstationary downscaling from the global atmospheric circulation to the local surges should be similar to upscaling the short scales of less than days to the scales of months, i.e. the upscaling in which the significant interaction between the surges and tides is more important

## 5. Conclusion

The results of the study explain key role of the climate patterns in the nonstationary dynamics of the extreme surges; the ‘switch on’ and ‘off’ of each cli-

mate index is strongly related to the multiscale variability. The use of the climate drivers could help improving the intermonthly and the interannual forecasting. Furthermore, they can be considered for GCM simulations that are designed to look for the physical mechanisms explaining the teleconnections between the atmospheric circulation and the sea-level variability.

Depending on the atmospheric circulation, described by the climate indices and weather forecasts, the stochastic models necessary for estimating the extreme surges can be developed and improved according with their multiscale variability and their physical connections with the global climate oscillations. Furthermore, similar assessments should be undertaken to improve understanding of the storminess uncertainty.

## Acknowledgments

The authors are grateful to the international project COTEST funded by CNES-TOSCA and related to the future mission of Surface Water and Ocean Topography (SWOT). Authors also would like to thank National Navy Hydrographic Service and National Center for Environmental Prediction for providing sea level and atmospheric data. Finally, the authors would like to express their gratitude to the editor and the unknown reviewers for the excellent suggestions, which improved the original manuscript.

## References

- Akaike, H., 1974. Information theory as an extension of the maximum likelihood principle. In: Petrov, B.N., Csaki, F. (Eds.), *Second International Symposium on Information Theory*. Akademiai Kiado, Budapest, 267–281.
- Andrade, C., Leite, S.M., Santos, J.A., 2012. Temperature extremes in Europe: overview of their driving atmospheric patterns. *Nat. Hazards Earth Syst. Sci.* 12, 1671–1691, <https://doi.org/10.5194/nhess-12-1671-2012>.
- Bell, R., Goring, G., D., G., 1998. Seasonal Variability of Sea Level and Sea-surface Temperature on the North-east Coast of New Zealand. *Estuar. Coast. Shelf. Sci.* 46 (2), 307–319, <https://doi.org/10.1006/ecss.1997.0286>.
- Bessoumoulin, P., 2002. Les tempêtes en France. *Annales des Mines* 9–14.
- Brown, J., Souza, A., Wolf, J., 2010. Surge modelling in the eastern Irish Sea: Present and future storm impact. *Ocean Dynam.* 60 (2), 227–236, <https://doi.org/10.1007/s10236-009-0248-8>.
- Colberg, F., McInnes, K.L., Grady, J., Hoeke, R., 2019. Atmospheric circulation changes and their impact on extreme sea levels around Australia. *Nat. Hazards Earth Syst. Sci.* 19, 1067–1086, <https://doi.org/10.5194/nhess-19-1067-2019>.
- Coleman, T.F., Li, Y., 1996. An interior trust region approach for nonlinear minimization subject to bounds. *SIAM J. Optim.* 6 (2), 418–445, <https://doi.org/10.1137/0806023>.
- Coles, S., 2001. *An Introduction to Statistical Modeling of Extreme Values*. Springer, London, 209 pp.
- Corte-Real, J., Zhang, Z., Wang, X., 1995. Large-scale circulation regimes and surface climatic anomalies over the Mediterranean. *Int. J. Climatol.* 15, 1135–1150, <https://doi.org/10.1002/joc.3370151006>.
- Costa, S., Cantat, O., Pirazzoli, P.A., Lemaitre, M., Delahaye, D., 2004. Vents forts et submersions de tempête en Manche Orientale: analyse météo-marine sur la période historique ré-

- cente. Actes du Colloque de l'Association Internationale de Climatologie. Climat, mémoire du temps. Les relations climat-espace-société, 277–280.
- Dangendorf, S., Wahl, T., Hein, H., Jensen, J., Mai, S., Mudersbach, C., 2012. Level Variability and Influence of the North Atlantic Oscillation on Long-Term Trends in the German Bight. *Water* 4 (1), 170–195, <https://doi.org/10.3390/w4010170>.
- Feliks, Y., Ghil, M., Robertson, A.W., 2011. The atmospheric circulation over the North Atlantic as induced by the SST field. *J. Clim.* 24 (2), 522–542, <https://doi.org/10.1175/2010JCLI3859.1>.
- Frankignoul, C., Sennechael, N., Kwon, Y.-O., Alexander, M.A., 2011. Influence of the Meridional Shifts of the Kuroshio and the Oyashio Extensions on the Atmospheric Circulation. *J. Climate* 24, 762–777, <https://doi.org/10.1175/2010JCLI3731.1>.
- Haigh, I., Nicolls, R., Wells, N., 2009. Mean sea level trends around the English Channel over the 20<sup>th</sup> century and their wider context. *Cont. Shelf. Res.* 29, 2083–2098, <https://doi.org/10.1016/j.csr.2009.07.013>.
- Haigh, I., Nicolls, R., Wells, N., 2010. Assessing changes in extreme sea levels: Application to the English Channel 1900–2006. *Cont. Shelf. Res.* 30, 1042–1055, <https://doi.org/10.1016/j.csr.2010.02.002>.
- Hanson, S., Nicholls, R., Ranger, N., Hallegatte, S., Dorfe-Morlot, J., Herweijer, C., Chateau, J., 2011. A global ranking of port cities with high exposure to climate extremes. *Clim. Change.* 104 (1), 89–111, <https://doi.org/10.1007/s10584-010-9977-4>.
- Idier, D., Dumas, F., Muller, H., 2012. Tide-surge interaction in the English Channel. *Nat. Hazards Earth Syst. Sci.* 12, 3709–3718, <https://doi.org/10.5194/nhess-12-3709-2012>.
- Idier, D., Paris, F., Le Cozannet, G., Boulahya, F., Dumas, F., 2017. Sea-level rise impacts on the tides of the European Shelf. *Cont. Shelf. Res.* 137, 56–71, <https://doi.org/10.1016/j.csr.2017.01.007>.
- Labat, D., 2005. Recent advances in wavelet analyses: Part 1. A review of concepts. *J. Hydrol.* 314 (1–4), 275–288, <https://doi.org/10.1016/j.jhydrol.2005.04.003>.
- Lavers, D.A., Hannah, D.M., Bradley, C., 2015. Connecting large-scale atmospheric circulation, river flow and groundwater levels in a chalk catchment in southern England. *J. Hydrol.* 523, 179–189, <https://doi.org/10.1016/j.jhydrol.2015.01.060>.
- Lavers, D.A., Prudhomme, C., Hannah, D.M., 2010. Large-scale climate, precipitation and British river flows: Identifying hydro-climatological connections and dynamics. *J. Hydrol.* 395 (3–4), 242–255, <https://doi.org/10.1016/j.jhydrol.2010.10.036>.
- Levin, S.A., 1992. The problem of pattern and scale in ecology: the Robert H. MacArthur Award Lecture. *Ecology* 73, 1943–1967.
- L'Heureux, M.L., Thompson, D.W.J., 2006. Observed relationships between the El Niño–Southern Oscillation and the extratropical zonal-mean circulation. *J. Climate.* 19, 276–287, <https://doi.org/10.1175/JCLI3617.1>.
- López-Parages, J., Rodríguez-Fonseca, B., 2012. Multidecadal modulation of El Niño influence on the Euro-Mediterranean rainfall. *Geophys. Res. Lett.* 39, art. 1009 no. L02704, <https://doi.org/10.1029/2011GL050049>.
- Lu, J., Chen, G., Frierson, D., M., W., 2008. Response of the Zonal Mean Atmospheric Circulation to El Niño versus Global Warming. *J. Climate* 21, 5835–5851, <https://doi.org/10.1175/2008JCLI2200.1>.
- Marcos, M., Chust, G., Jordá, G., Caballero, A., 2012. Effect of sea level extremes on the western Basque coast during the 21st century. *Clim. Res.* 51 (3), 237–248, <https://doi.org/10.3354/cr01069>.
- Masina, M., Lamberti, A., 2013. A nonstationary analysis for the Northern Adriatic extreme sea levels. *J. Geophys. Res.* 118, 3999–4016, <https://doi.org/10.1002/jgrc.20313>.
- Massei, N., Dieppois, B., Hannah, D.M., Lavers, D.A., Fossa, M., Laignel, B., Debret, M., 2017. Multi-time-scale hydroclimate dynamics of a regional watershed and links to large-scale atmospheric circulation: Application to the Seine river catchment. France. *J. Hydrol.* 546, 262–275, <https://doi.org/10.1016/j.jhydrol.2012.04.052>.
- Mayes, J., Wheeler, D., 2013. Regional weather and climates of the British Isles - Part 1: Introduction. *Weather* 68 (1), 3–8, <https://doi.org/10.1002/wea.2041>.
- Menendez, M., Woodworth, P.L., 2010. Changes in extreme high water levels based on a quasi-global tide-gauge data set. *J. Geophys. Res.* 115, art. no. C10011, <https://doi.org/10.1029/2009JC005997>.
- Mizuta, R., 2012. Intensification of extratropical cyclones associated with the polar jet change in the CMIP5 global warming projections. *Geophys. Res. Lett.* 39, 1–6. art. no. L19707, <https://doi.org/10.1029/2012GL053032>.
- Nakamura, M., Yamane, S., 2009. Dominant anomaly patterns in the near-surface baroclinicity and accompanying anomalies in the atmosphere and oceans. Part I: North Atlantic basin. *J. Climate* 22, 880–904, <https://doi.org/10.1175/2010JCLI3017.1>.
- Namias, J., 1969. On the causes of the small number of Atlantic hurricanes in 1968. *Mon. Weather Rev.* 97 (4), 346–348.
- Nicholls, R.J., Marinova, N., Lowe, J.A., Brown, S., Vellinga, P., De Gusmao, D., Hinkel, J., Tol, R.S., 2011. Sea-level rise and its possible impacts given a “beyond 4 C world” in the twenty-first century. *Philos. T. Roy. Soc. A* 369, 161–181, <https://doi.org/10.1098/rsta.2010.0291>.
- O'Reilly, C.H., Czaja, A., 2015. The response of the Pacific storm track and atmospheric circulation to Kuroshio Extension variability. *Q. J. Roy. Meteor. Soc.* 141 (686), 52–66, <https://doi.org/10.1002/qj.2334>.
- Pasquini, A.I., Lecomte, K.L., Depetris, P.J., 2008. Climate change and recent water level variability in Patagonian proglacial lakes, Argentina. *Global Planet. Change* 63, 290–298.
- Philips, M.R., Rees, E.F., Thomas, T., 2013. winds, sea level and North Atlantic Oscillation (NAO) influences: An evaluation; *Global Planet. Change* 100, 145–152, <https://doi.org/10.1016/j.gloplacha.2012.10.01>.
- Pirazzoli, P.A., 2005. A review of possible eustatic, isostatic and tectonic contributions in eight late-Holocene relative sea-level histories from the Mediterranean area. *Quaternary Sci. Rev.* 24 (18–19), 1989–2001, <https://doi.org/10.1016/j.quascirev.2004.06.026>.
- Pugh, D.J., 1987. *Tides, Surges and Mean Sea-Level: A Handbook for Engineers and Scientists*. John Wiley, Chichester 472 pp.
- Sang, Y.F., 2013. A review on the applications of wavelet transform in hydrology time series analysis. *Atmos. Res.* 122, 8–15, <https://doi.org/10.1016/j.atmosres.2012.11.003>.
- Schlesinger, M.E., Ramankutty, N., 1994. An oscillation in the global climate system of period 65–70 years. *Nature* 367, 723–726.
- Seager, R., Harnik, N., Kushnir, Y., Robinson, W., Miller, J., 2003. Mechanisms of hemispherically symmetric climate variability. *J. Climate* 16, 2960–2978.
- Shaw, A.G.P., Tsimplis, M.N., 2010. The 18.6 yr nodal modulation in the tides of Southern European Coasts. *Cont. Shelf Res.* 30 (2), 138–151, <https://doi.org/10.1016/j.csr.2009.10.006>.
- SHOM, 2014. Caractérisation de 7 évènements de tempêtes de l'automne-hiver 2013–2014 N°001/2014.
- Small, R.J., Tomas, R.A., Bryan, F.O., 2014. Storm track response to ocean fronts in a global high-resolution climate model. *Clim. Dynam.* 43, 805–828, <https://doi.org/10.1007/s00382-013-1980-9>.
- Tomasin, A., Pirazzoli, P.A., 2008. Extreme Sea Levels in the English Channel: Calibration of the Joint Probability Method. *J. Coastal Res.* 24, 1–13, <https://doi.org/10.2112/07-0826.1>.

- Torrence, C., Compo, G.P., 1998. A practical guide to wavelet analysis. *B. Am. Meteorol. Soc.* 79, 61–78, [https://doi.org/10.1175/1520-0477\(1998\)079<0061:APGTWA>0.CO;2](https://doi.org/10.1175/1520-0477(1998)079<0061:APGTWA>0.CO;2).
- Trigo, R.M., Osborn, T.J., Corte-Real, J., 2002. The North Atlantic Oscillation influence on Europe: climate impacts and associated physical mechanisms. *Clim. Res.* 20, 9–17, <https://doi.org/10.3354/cr020009>.
- Trisimplis, M.N., Josey, S.A., 2001. Forcing of the Mediterranean Sea by atmospheric oscillations over the North Atlantic. *Geophys. Res. Lett.* 28, 803–806.
- Tsimplis, M.N., Woodworth, P.L., 1994. The global distribution of the seasonal sea level cycle calculated from coastal tide gauge data. *J. Geophys. Res.* 99 (C8), 16031–16039.
- Turki, I., Laignel, B., Chevalier, L., Massei, N., Costa, S., 2015b. On the Investigation of the Sea Level Variability in Coastal Zones using SWOT Satellite Mission: example of the Eastern English Channel (Western France). *IEEE J. Sel. Top. Appl.* 8 (4), 1564–1569, <https://doi.org/10.1109/JSTARS.2015.2419693>.
- Turki, I., Laignel, B., Kakeh, N., Chevalier, L., Costa, S., 2015a. Methodology for Filling gaps and Forecast in sea level: application to the eastern English Channel and the North Atlantic Sea (western France). *Ocean Dynam.* 65 (9–10), 1221–1234, <https://doi.org/10.1007/s10236-015-0824-z>.
- Turki, I., Massei, N., Laignel, B., 2019. Linking Sea Level Dynamic and Exceptional Events to Large-scale Atmospheric Circulation Variability: Case of Seine Bay, France. *Oceanologia* 61 (3), 321–330, <https://doi.org/10.1016/j.oceano.2019.01.003>.
- Vousdoukas, M.I., Mentaschi, L., Voukouvalas, E., Verlaan, M., Feyen, L., 2017. Extreme sea levels on the rise along Europe's coasts. *Earth's Future* 5 (3), 304–323, <https://doi.org/10.1002/2016EF000505>.
- Wang, C., 2001. Atlantic Climate Variability and Its Associated Atmospheric Circulation Cells. *J. Climate* 15, 1516–1536.
- Williams, J., Irazoqui Apecechea, M., Sauter, A., Horsburgh, K.J., 2018. Radiational tides: their double-counting in storm surge forecasts and contribution to the Highest Astronomical Tide. *Ocean Sci.* 14, 1057–1068, <https://doi.org/10.5194/os-14-1057-2018>.
- Wills, S.W., Thompson, D.W.J., Ciasto, L.M., 2016. On the Observed Relationships between Variability in Gulf Stream Sea Surface Temperatures and the Atmospheric Circulation over the North Atlantic. *J. Climate* 29, 3719–3730, <https://doi.org/10.1175/JCLI-D-15-0820.1>.
- Yan, Z., Tsimplis, M.N., Woolf, D., 2004. Analysis of the relationship between the North Atlantic Oscillation and sea-level changes in northwestern Europe. *Int. J. Climatol.* 24, 743–758, <https://doi.org/10.1002/joc.1035>.
- Zampieri, M., Toreti, A., Schindler, A., Escocciarro, E., Gualdi, S., 2017. Atlantic multi-decadal oscillation influence on weather regimes over Europe and the Mediterranean in spring and summer. *Global Planet. Change*, 151, 92–100, <https://doi.org/10.1016/j.gloplacha.2016.08.014>.
- Zappa, G., Shaffrey, L.C., Hodges, K.I., Sansom, P., Stephenson, D.B., 2013. A multimodel assessment of future projections of North Atlantic and European cyclones in the CMIP5 climate models. *J. Climate* 26, 5846–5862, <https://doi.org/10.1175/JCLI-D-12-00573.1>.